Emerald Insight

Engineering Computations

2D particle contact-based meshfree method in CDEM and its application in geotechnical problems

Chun Feng Shi-hai Li Eugenio Onate

Article information:

To cite this document:
Chun Feng Shi-hai Li Eugenio Onate , (2015),"2D particle contact-based meshfree method in CDEM and its application in geotechnical problems", Engineering Computations, Vol. 32 Iss 4 pp. 1080 - 1103
Permanent link to this document:
http://dx.doi.org/10.1108/EC-04-2014-0095

Downloaded on: 26 February 2016, At: 00:52 (PT)
References: this document contains references to 25 other documents.
To copy this document: permissions@emeraldinsight.com
The fulltext of this document has been downloaded 85 times since 2015*

Users who downloaded this article also downloaded:

Shunying Ji, Shaocheng Di, Shewen Liu, (2015),"Analysis of ice load on conical structure with discrete element method", Engineering Computations, Vol. 32 Iss 4 pp. 1121-1134 http://dx.doi.org/10.1108/EC-04-2014-0090

Wei Zhou, Gang Ma, Xiao-Lin Chang, Yin Duan, (2015),"Discrete modeling of rockfill materials considering the irregular shaped particles and their crushability", Engineering Computations, Vol. 32 Iss 4 pp. 1104-1120 http://dx.doi.org/10.1108/EC-04-2014-0086

Yuanqiang Tan, Rong Deng, Y T Feng, Hao Zhang, Shengqiang Jiang, (2015),"Numerical study of concrete mixing transport process and mixing mechanism of truck mixer", Engineering Computations, Vol. 32 Iss 4 pp. 1041-1065 http://dx.doi.org/10.1108/EC-04-2014-0097

Access to this document was granted through an Emerald subscription provided by emerald-srm:380560 []

For Authors

If you would like to write for this, or any other Emerald publication, then please use our Emerald for Authors service information about how to choose which publication to write for and submission guidelines are available for all. Please visit www.emeraldinsight.com/authors for more information.

About Emerald www.emeraldinsight.com

Emerald is a global publisher linking research and practice to the benefit of society. The company manages a portfolio of more than 290 journals and over 2,350 books and book series volumes, as well as providing an extensive range of online products and additional customer resources and services.

Downloaded by Kungliga Tekniska Högskolan At 00:52 26 February 2016 (PT)

Emerald is both COUNTER 4 and TRANSFER compliant. The organization is a partner of the Committee on Publication Ethics (COPE) and also works with Portico and the LOCKSS initiative for digital archive preservation.

*Related content and download information correct at time of download.

Downloaded by Kungliga Tekniska Högskolan At 00:52 26 February 2016 (PT)

The current issue and full text archive of this journal is available on Emerald Insight at:
www.emeraldinsight.com/0264-4401.htm

Received 24 April 2014
Revised 27 June 2014
Accepted 27 June 2014

Downloaded by Kungliga Tekniska Högskolan At 00:52 26 February 2016 (PT)

2D particle contact-based meshfree method in CDEM and its application in geotechnical problems

Chun Feng and Shi-hai Li
Key Laboratory for Mechanics in Fluid Solid Coupling Systems, Institute of Mechanics, Chinese Academy of Sciences, Beijing, China, and
Eugenio Onate
International Centre for Numerical Methods in Engineering, Universitat Politècnica de Catalunya, Barcelona, Spain

Abstract

Purpose – Continuum-based discrete element method is an explicit numerical method, which is a combination of block discrete element method (DEM) and FEM. When simulating large deformation problems, such as cutting, blasting, water-like material flowing, the distortion of elements will lead to no convergence of the numerical system. To solve the convergence problem, a particle contact-based meshfree method (PCMM) is introduced in. The paper aims to discuss this issue.

Design/methodology/approach – PCMM is based on traditional particle DEM, and use particle contacts to generate triangular elements. If three particles are contact with each other, the element will be created. Once elements are created, the macroscopic constitutive law could be introduced in. When large deformation of element occurs, the contact relationship between particles will be changed. Those elements that do not meet the contact condition will be deleted, and new elements that coincide with the relationship will be generated. By the deletion and creation of elements, the convergence problem induced by element distortion will be eliminated. To solve FEM and PCMM coupled problems, a point-edge contact model is introduced in, and normal and tangential springs are adopted to transfer the contact force between particles and blocks.

Findings – According to the deletion and recreation of elements based on particle contacts, PCMM could simulate large deformation problems. Some numerical cases (i.e. elastic field testing, uniaxial compression analysis and wave propagation simulation) show the accuracy of PCMM, and others (i.e. soil cutting, contact burst and water-like material flowing) show the rationality of PCMM.

Originality/value – In traditional particle DEM, contact relationships are used to calculate contact forces. But in PCMM, contact relationships are adopted to generate elements. Compared to other meshfree methods, in PCMM, the element automatic deletion and recreation technique is used to solve large deformation problems.

Keywords Numerical simulation, Cutting, Meshfree method, Particle contact, PCMM, Rock and soil

Paper type Research paper

1. Introduction

Continuum-based discrete element method (CDEM) is an explicit numerical method. Due to its combination of block discrete element method (DEM) and FEM, the

The authors would like to thank the support from the National Basic Research Program of the Ministry of Science and Technology of China (Grant No. 2010CB731506), the National Key Technology Research and Development Program of the Ministry of Science and Technology of China (Grant No. 2012BAK10B01) and the Youth Science Fund of National Natural Science Foundation of China (Grant No. 11302230).

Engineering Computations: International Journal for Computer-Aided Engineering and Software
Vol. 32 No. 4, 2015
pp. 1080-1103
© Emerald Group Publishing Limited
0264-4401
DOI 10.1108/EC-04-2014-0095

Downloaded by Kungliga Tekniska Högskolan At 00:52 26 February 2016 (PT)

progressive failure of geological body could be simulated well (Wang *et al.*, 2005; Li *et al.*, 2004, 2007; Ma *et al.*, 2011a, b). But when simulating some large deformation problems, such as cutting, blasting, water-like material flowing, the numerical system will become instable due to the serious distortion of elements. To eliminate this problem, a particle contact-based meshfree method (PCMM) is introduced in.

The convergence problem induced by grid distortion is a traditional topic in FEM in Lagrangian description. Generally speaking, any numerical methods which use elements to calculate deformation force in Lagrangian coordinate system will meet the problem. To eliminate the problem, adaptive remeshing procedures are good choices (Littlefield, 2001; Oñate *et al.*, 2004). However, it is generally tedious and time consuming, and may introduce additional inaccuracy into the solution.

Another choice to solve mesh distortion is to describe material flow through a fixed grid in space in Euler system, but the dissipation problem associated with mass flux between adjacent elements will arise. Besides, it is difficult to catch the material interface, although the level set or volume of fluid method could solve the problem to some extent. Recently, there are some mixed methods to strengthen the advantages of Lagrangian and Eulerian descriptions and to avoid their disadvantages, such as arbitrary Lagrangian-Eulerian (ALE) (Liu *et al.*, 1986, 1991). Unfortunately, the convective transport effect in ALE often leads to spurious oscillation that needs to be stabilized by artificial diffusion or Petrov-Galerkin stabilization.

These years, a strong interest is focussed on meshfree methods, and these methods are expected to be superior to the conventional grid-based FEM or finite volume method (FVM) for many applications. The key idea of the meshfree methods is to provide accurate and stable numerical solutions for integral equations with all kinds of possible boundary conditions with a set of arbitrarily nodes or particles, so that the difficulties associated with mesh distortion can be avoided or alleviated. Nevertheless, most of meshfree methods suffer from higher computational cost and the accuracy of some meshfree methods is still dependent on the node regularities to some extent. Therefore, only a few of them perform well in large deformation simulation, such as smoothed particle hydrodynamics (SPH) and material point method (MPM).

SPH is one of the earliest particle methods, which was proposed by Lucy (1977) and Gingold (Gingold and Monaghan, 1977) simultaneously in 1977 for solving astrophysical problems. The basic idea of SPH is to approximate field quantities by kernel function in a smoothing length. According to the differentiation and integration of kernel function, the differentiation and integration of spatial field quantities could be obtained. Nowadays, SPH and its improved versions have been successfully applied in many fields, such as free surface fluid flow (Cleary *et al.*, 2006), hypervelocity impact (Michel *et al.*, 2006) and progressive failure of geological body (Ma *et al.*, 2011a, b). However, due to the normalization and compact of kernel function, some errors will occur when particles locate on or near the boundaries (Ma *et al.*, 2009), although there are some methods to solve the problem (Campbell, 1989; Randles and Libersky, 2000). Furthermore, SPH converts the integration over the support domain into a summation only over a finite number of particles, so insufficient sampling points for integration may result in numerical instability. When particles are under tensile stress state, the motion of the particles become unstable, and that may lead to particle clumping or complete blowup in the computation (Swegle *et al.*, 1995). Recently, some improved methods are suggested to solve the tensile instability, such as corrective smoothed particle method (Chen *et al.*, 1999), artificial force (Monaghan, 2000) and stress points (Dyka *et al.*, 1997).

Downloaded by Kungliga Tekniska Högskolan At 00:52 26 February 2016 (PT)

MPM (Sulsky *et al.*, 1994, 1995) is a finite element-based particle method, which is evolved from particle in cell method (Brackbill and Ruppel, 1986). In MPM, material domain is discretized by a group of points, termed as particles or material points. These Lagrangian particles carry all material information and track the deformation history. The momentums equations are solved on a predefined background grid, which can be fixed in space or arbitrarily defined, and provide an Eulerian description of the material domain (Ma *et al.*, 2009). Compared with SPH, MPM owns higher accuracy, better computational stability and lower computational time consuming. However, the density of material points used in computation will influence the computational results (Ambati *et al.*, 2012).

In this paper, a PCMM is introduced. In Section 2, the basic principles of PCMM are introduced; in Section 3, some simple numerical cases are presented to show the accuracy of PCMM; and in Section 4, the numerical cases in geotechnical problems are shown to demonstrate the rationality of this method.

2. Principles of PCMM

2.1 Main idea

Contact pairs searching and contact forces calculation are two main steps in DEM. Due to the abundant information in contact pairs, the elements which are used to calculate deformation force could be formed easily.

PCMM is the method which uses the contact pairs of DEM to generate the elements and uses the elements to simulate engineering problems. By renewing neighbors for each particle in each step, the elements will be created or deleted correspondingly, and then the element distortion problems will be solved automatically. Figure 1 shows the main idea of PCMM.

Incremental-based explicit method is adopted for PCMM, and forward-difference approximation is used. In PCMM, all the field variables (i.e. stress, strain, density, acceleration, velocity and displacement) are stored in particles. Particles are adopted to

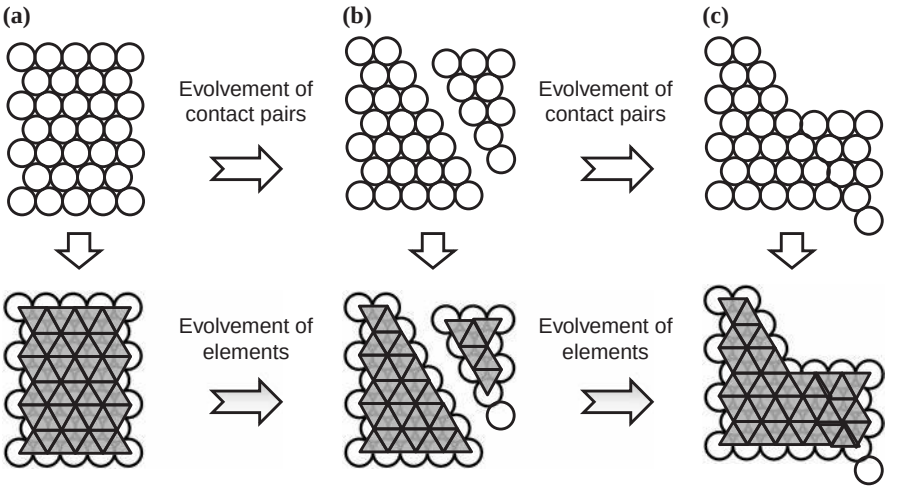

Figure 1.
Main idea of PCMM

Notes: (a) Elements creation based on particle contacts; (b) elements deletion; (c) elements recreation

compute movement, and elements are used to calculate deformation force. Several steps should be repeated in each time step:

(1) Neighbor deletion: delete neighbors which do not contact with the particle.

(2) Neighbor searching: find neighbors for each particle.

(3) Element deletion: delete elements which do not satisfy corresponding condition.

(4) Element creation: create elements based on new neighbor relationship.

(5) Deformation force calculation: based on continuous constitutive law, calculate stress and node force.

(6) Contact force calculation: if particle-block contact exists, calculate the contact force.

(7) Particle evolvement calculation: based on Newton's law, calculate the movement of each particle.

2.2 Elements creation

In PCMM, the element type is triangle element. For creating triangle elements, three conditions should be satisfied at the same time: first, the three particles of which the triangle element consists should contact with each other (Equation (1)); second, to ensure the quality of elements, each internal angle of the triangle element should be between 30 and 150 degree (Equation (2)); and third, each edge length of the element should be larger than 0.5 times of average radius of three particles (Equation (3)). Where $\boldsymbol{R_i}$ denotes the radius of particle $\boldsymbol{i}$, $\boldsymbol{d_{ij}}$ means the distance between particle $\boldsymbol{i}$ and $\boldsymbol{j}$, $\boldsymbol{\theta_i}$ is the internal angle and $\boldsymbol{\delta}$ means the tolerance for contact searching:

$$\begin{cases} d_{ij} \leqslant R_i + R_j + \delta \\ i = 1,2,3; j = 1,2,3; i \neq j \end{cases} \tag{1}$$

$$30^\circ \leqslant \theta_i \leqslant 150^\circ \quad i = 1,2,3 \tag{2}$$

$$\begin{cases} d_{ij} \geqslant 0.5 \times \frac{R_1 + R_2 + R_3}{3} \\ i = 1,2,3; j = 1,2,3; i \neq j \end{cases} \tag{3}$$

For setting up good element system, especially based on a series of random particles, $\boldsymbol{\delta}$ should be large enough to avoid gaps. In Figure 2, with small $\boldsymbol{\delta}$, only triangle elements **T136**, **T356** and **T345** will be formed; while with large $\boldsymbol{\delta}$, triangle elements **T136**, **T356**, **T345**, **T123** and **T234** will be created.

For searching contact pairs and creating elements easier, the corresponding contact linked-lists and element linked-lists are stored in each particle. To search particle contact pairs efficiently, static bin is adopted and 2D bin array is created (Figure 3). The host cell (X3, Y3) of host particle $\boldsymbol{A}$ should be located first, and then neighbor search will be executed on surrounding nine cells, from (X2, Y2) to (X4, Y4).

If particle $\boldsymbol{i}$ is the neighbor of host particle $\boldsymbol{A}$, adds particle $\boldsymbol{i}$ to the contact linked-list of $\boldsymbol{A}$. After finishing neighbor search for particle $\boldsymbol{A}$, calculates the position angle for

Downloaded by Kungliga Tekniska Högskolan At 00:52 26 February 2016 (PT)

each contact pairs, then sequences the neighbors based on the position angle (anticlockwise sequencing scheme is adopted). If the included angle between two adjacent neighbors is smaller than 30 degree, the neighbor which is farther from host particle $\boldsymbol{A}$ should be deleted from contact linked-list (Figure 4).

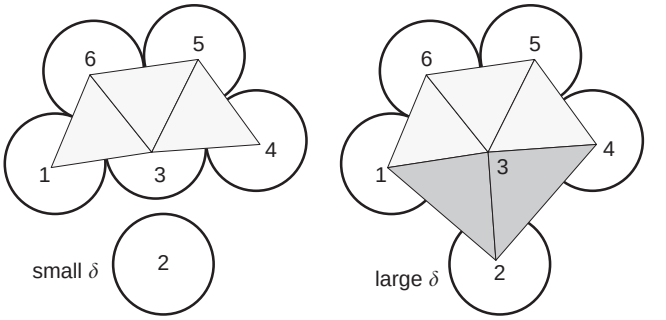

Figure 2.
Different element systems due to different $\boldsymbol{\delta}$

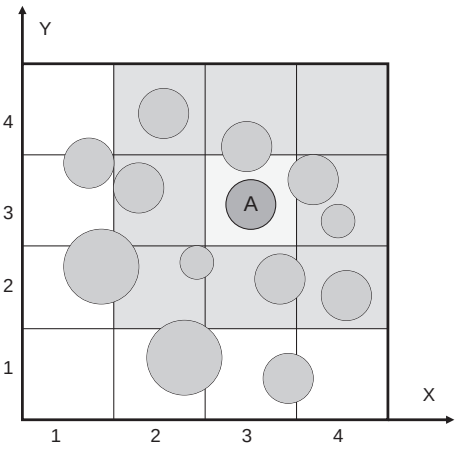

Figure 3.
Bin array for neighbor searching

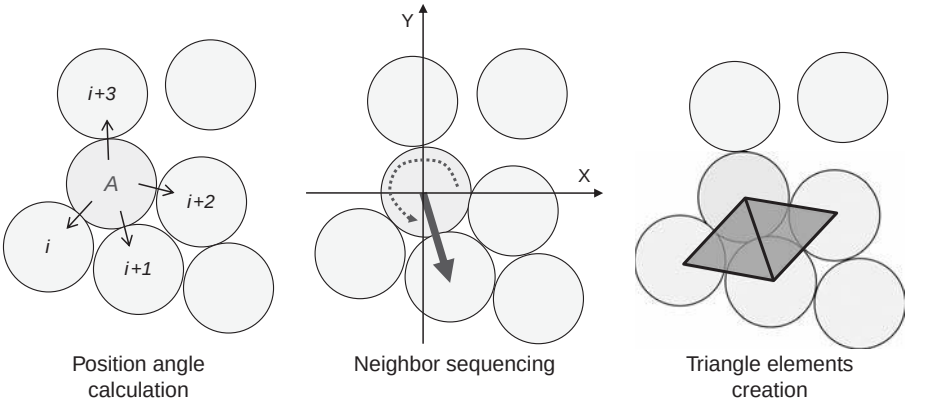

Figure 4.
Neighbor sequencing and element creation according to position angle

Downloaded by Kungliga Tekniska Högskolan At 00:52 26 February 2016 (PT)

Downloaded by Kungliga Tekniska Högskolan At 00:52 26 February 2016 (PT)

After sequencing and deleting neighbors which are mentioned above, loops the contact linked-list of host particle $\boldsymbol{A}$ and checks if particle $\boldsymbol{A}$, $\boldsymbol{i}$ and $\boldsymbol{i+1}$ could form a triangle element. If the quasi-element satisfies Equations (1)-(3), and it is a new element (does not exist in element linked-list), adds this element to the element linked-list of particle $\boldsymbol{A}$ (Figure 4).

After finishing contact linked-lists creation and element linked-lists generation, the element system based on contact pairs is generated.

2.3 Superposition algorithm

Based on element creating strategy and storing mechanism mentioned in Section 2.2, overlapping elements will be created. If three particles contact with each other (Figure 5(a)), three overlapping elements will be created, which are **T123** stored in particle **1**, **T231** stored in particle **2** and **T312** stored in particle **3**. If four particles contact with each other (Figure 5(b)), eight overlapping elements will be created, which are **T123** and **T143** stored in particle **1**, **T214** and **T234** stored in particle **2**, **T321** and **T341** stored in particle **3** and **T432** and **T412** stored in particle **4**. If five particles contact with each other (Figure 5(c)), 15 elements will be created, which are **T123**, **T134** and **T145** stored in particle **1**, **T234**, **T245** and **T251** stored in particle **2**, **T345**, **T351** and **T312** stored in particle **3**, **T451**, **T412** and **T423** stored in particle **4** and **T512**, **T523** and **T534** stored in particle **5**. In 3-particle cluster, the cluster domain **D123** is overlapped three times; in four-particle cluster, the cluster domain **D1234** is overlapped four times; and in five-particle cluster, the cluster domain **D12345** is overlapped five times.

To solve above mentioned overlapping problems, superposition algorithm is adopted. That means, when calculate element deformation force, the contribution of each element should be divided by particle number in a given cluster (Equation (4)). Where, $\boldsymbol{N}$ means the number of particles which contact with each other, F_r^i denotes the real deformation force contributed by element $\boldsymbol{i}$, and F_v^i means the virtual deformation force of element $\boldsymbol{i}$:

$$F_r^i = \frac{F_v^i}{N} \tag{4}$$

For simulating continuous problems well, the masses of particles in PCMM are obtained from cluster domain (Equation (5)). Where, $\boldsymbol{M_i}$ denotes the mass of particle

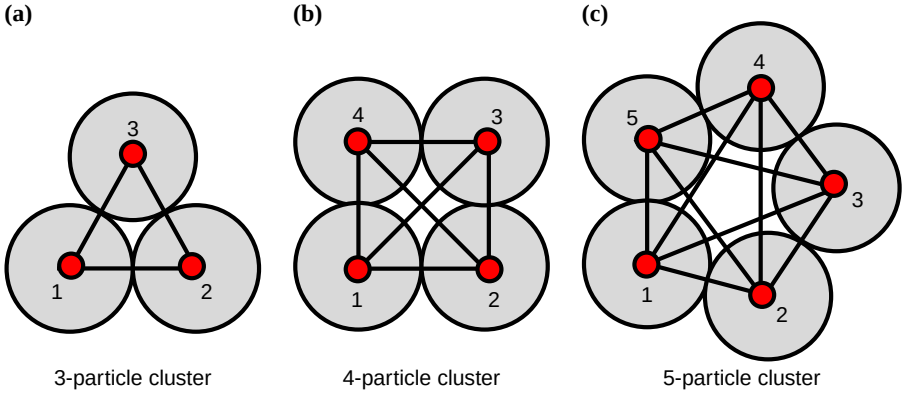

Figure 5.
Different particle clusters

Downloaded by Kungliga Tekniska Högskolan At 00:52 26 February 2016 (PT)

i, ρ_j means the density of cluster domain j, S_j represents the volume of cluster domain j in 2D, N_j is the particle number of cluster domain j, and H denotes the total cluster number related to particle i:

$$M_i = \sum_{j=0}^{H} \frac{\rho_j S_j}{N_j} \tag{5}$$

2.4 Element stress and deformation force calculation

Incremental-based FVM is adopted (Jing and Stephansson, 2007) to calculate element stress and deformation force. In numerical time t_0, particle velocity could be gotten from Newton's law, and the velocity gradient of each triangle element could be obtained by Gauss's theorem (Equation (6)). Where $\langle \partial v_i / \partial x_j \rangle$ means the average velocity gradient of element, S_e denotes the volume of element in 2D, $\overline{v}_i$ represents the average velocity in edge k, n_j^k is the jth component of unit normal vector in edge k and ΔL^k is the length of edge k.

$$\frac{\partial v_i}{\partial x_j} \approx \left\langle \frac{\partial v_i}{\partial x_j} \right\rangle = \frac{1}{S_e} \sum_{k=1}^{3} \overline{v_i} n_j^k \Delta L^k \tag{6}$$

Based on Equation (6), incremental strain of the element could be calculated (Equation (7)), where $\Delta \varepsilon_{ij}$ denotes element incremental strain, and Δt means time step:

$$\Delta \varepsilon_{ij} = \frac{1}{2} \left(\frac{\partial v_i}{\partial x_j} + \frac{\partial v_j}{\partial x_i} \right) \Delta t \tag{7}$$

According to Equations (8) and (9), the stress increment $\Delta \sigma_{ij}$ and the stress σ_{ij} could be gotten. Where K denotes bulk modulus, G means shear modulus, $\Delta \theta$ means incremental bulk strain, δ_{ij} is Kronecker delta and $\sigma_{ij\text{-}old}$ is element stress in last step. $\Delta \theta$ could be obtained by Equation (10), and $\sigma_{ij\text{-}old}$ could be calculated by Equation (11). Where, σ_{ij-old}^{p1}, σ_{ij-old}^{p2} and σ_{ij-old}^{p3} are the stresses of three particles in last step:

$$\Delta \sigma_{ij} = 2G \Delta \varepsilon_{ij} + \left(K - \frac{2}{3} G \right) \Delta \theta \delta_{ij} \tag{8}$$

$$\sigma_{ij} = \Delta \sigma_{ij} + \sigma_{ij-old} \tag{9}$$

$$\Delta \theta = \Delta \varepsilon_{11} + \Delta \varepsilon_{22} + \Delta \varepsilon_{33} \tag{10}$$

$$\sigma_{ij-old} = \left(\sigma_{ij-old}^{p1} + \sigma_{ij-old}^{p2} + \sigma_{ij-old}^{p3} \right) / 3 \tag{11}$$

If some plastic constitutive law is adopted, the stress will be corrected. In this paper, maximum tensile criteria and Mohr-Coulomb criteria are adopted (Equation (12)).

Where $\boldsymbol{\sigma_{ij\text{-}new}}$ is corrected element stress in this step, $\boldsymbol{T}$, $\boldsymbol{C}$ and ϕ denote tensile strength, cohesion and inner friction angle:

$$\sigma_{ij-new} = f\left(\sigma_{ij}, T, C, \phi\right) \tag{12}$$

According to corrected stress tenser $\boldsymbol{\sigma_{ij\text{-}new}}$, the deformation force of the element could be calculated by Equation (13), where F_i^p means the $\boldsymbol{i}$th component of deformation force of node $\boldsymbol{p}$ (particle $\boldsymbol{p}$) in triangle element (each node owns two corresponding edges):

$$F_i^p = \sigma_{ij-new} \sum_{k=1}^{2} \left(n_j^k \Delta L^k / 2\right) \tag{13}$$

Due to the superposition algorithm described in Section 2.3, if a particle cluster contains $\boldsymbol{N}$ particles, the contributions of related elements should be divided by $\boldsymbol{N}$ (Equation (14)):

$$F_i^p = \frac{1}{N} \sigma_{ij-new} \sum_{k=1}^{2} \left(n_j^k \Delta L^k / 2\right) \tag{14}$$

After all the stresses and deformation forces of elements have been calculated, the element strains and stresses should be transformed to particles (Equations (15) and (16)). Where ε_{ij-new}^p and σ_{ij-new}^p denote particle strain and stress in this step, ε_{ij-old}^p means particle strain in last step, $\Delta\varepsilon_{ij-new}^k$ and σ_{ij-new}^k mean $\boldsymbol{k}$th element strain increment and stress in this step, and $\boldsymbol{M}$ represents the element number related to the particle:

$$\varepsilon_{ij-new}^p = \sum_{k=1}^{M} \Delta\varepsilon_{ij-new}^k / M + \varepsilon_{ij-old}^p \tag{15}$$

$$\sigma_{ij-new}^p = \sum_{k=1}^{M} \sigma_{ij-new}^k / M \tag{16}$$

2.5 Elements deletion

After some steps, element deformation will occur. If the deformation continues, the distortion will happen. To avoid element distortion, elements should be deleted if any condition mentioned below is satisfied:

(1) three particles of the triangle element do not contact with each other;

(2) any internal angle of the triangle element is smaller than 30 degree or larger than 150 degree; and

(3) any edge length of the element is smaller than 0.5 times of average radius of three particles.

According to Section 2.4, incremental method is used in PCMM, and all the variables (i.e. stress, strain, mass and velocity) are stored in particles. When uses element to compute deformation force, element strain and stress in last step are obtained from

Downloaded by Kungliga Tekniska Högskolan At 00:52 26 February 2016 (PT)

Downloaded by Kungliga Tekniska Högskolan At 00:52 26 February 2016 (PT)

particles by average algorithm, and element strain increment in this step is gotten from particle velocity by FVM. Based on the element strain, stress in last step and strain increment in this step, the new element strain and stress in this step could be computed, and the deformation force could be calculated. After that, strain, stress and resultant force of particles in this step will be obtained from the corresponding elements. Considering that strain energy, kinetic energy and potential energy are all stored in particles, element deletion will not cause the loss of force equilibrium, or the breakage of momentum/energy conservation.

2.6 Point-edge contact force calculation

In PCMM, for computing contact force between particles and blocks, the point-edge contacts should be set up (Figure 6). If the distance (Equation (17)) between particle $\boldsymbol{P}$ and edge $\boldsymbol{ij}$ is smaller than radius of particle ($\boldsymbol{d_{ij} < R}$) and the projection point of particle lies in the edge ($\boldsymbol{d_{ik} \leqslant d_{ij}}$, $\boldsymbol{d_{jk} \leqslant d_{ij}}$), the point-edge contact with one normal spring and one tangential spring will be created. Where $\overrightarrow{V}_{pi}$ denotes the position vector, $\overrightarrow{n}$ is the outer normal vector of edge $\boldsymbol{ij}$. The weighted coefficient of edge $\boldsymbol{ij}$ could be calculated by Equation (18):

$$d = \left| \overrightarrow{V}_{pi} \cdot \overrightarrow{n} \right| \tag{17}$$

$$\begin{cases} w_i = d_{jk}/d_{ij} \\ w_j = d_{ik}/d_{ij} \end{cases} \tag{18}$$

When calculating contact force, incremental method is adopted, and some steps should be followed:

(1) calculate relative incremental displacement (Equation (19)), where $\vec{v_p}$, $\vec{v_i}$ and $\vec{v_j}$ denote the velocity of particle $\boldsymbol{p}$, and the velocity of node $\boldsymbol{i}$ and node $\boldsymbol{j}$ of element:

$$\vec{d_g} = \left[\vec{v_p} - \left(w_i \vec{v_i} + w_j \vec{v_j} \right) \right] \Delta t \tag{19}$$

(2) convert $\vec{d_g}$ to local coordinate system (Equation (20)), where $[\boldsymbol{T}]$ denotes coordinate transformation matrix:

$$\vec{d_l} = [T] \vec{d_g} \tag{20}$$

(3) calculate contact force in local coordinate system (Equation (21)), where $\boldsymbol{K_n}$ and $\boldsymbol{K_s}$ represent the normal and tangential stiffness, $\boldsymbol{F_n}$ and $\boldsymbol{F_s}$ denote normal and

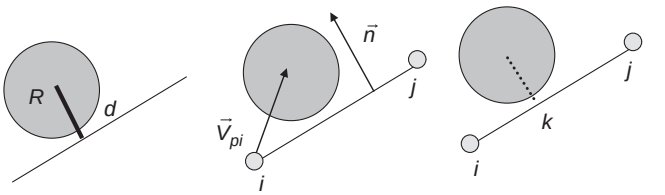

Figure 6.
Point-edge contact

tangential contact force in this step, $\boldsymbol{F_{n\text{-}old}}$ and $\boldsymbol{F_{s\text{-}old}}$ are contact force in last step, $\boldsymbol{\Delta d_{l\text{-}n}}$ and $\boldsymbol{\Delta d_{l\text{-}s}}$ are normal and tangential relative incremental displacement in local coordinate system:

$$\begin{cases} F_n = F_{n-old} - K_n \Delta d_{l-n} \\ F_s = F_{s-old} - K_s \Delta d_{l-s} \end{cases} \tag{21}$$

(4) correct contact force by maximum tensile criteria and Mohr-Coulomb criteria (Equation (22)), where $\boldsymbol{A}$ means contact area:

$$\begin{cases} (1)\, If\ -F_n \geqslant T \cdot A\ F_n = F_s = 0 \\ next\ step\ C = 0, T = 0 \\ (2)\, If\ F_s \geqslant F_n \times \tan(\phi) + C \cdot A \\ F_s = F_n \times \tan(\phi) + C \cdot A, \\ next\ step\ C = 0, T = 0 \end{cases} \tag{22}$$

(5) convert local contact force to global coordinate system (Equation (23)):

$$\vec{F_g} = [T]^T \vec{F_l} \tag{23}$$

(6) accumulate contact force to particles and edges (Equation 24), where $\vec{F_{p-new}}$, $\vec{F_{i-new}}$ and $\vec{F_{j-new}}$ mean contact force vector of particle $\boldsymbol{p}$, node $\boldsymbol{i}$ and node $\boldsymbol{j}$ in this step, and $\vec{F_{p-old}}$, $\vec{F_{i-old}}$ and $\vec{F_{j-old}}$ denote contact force vector of particle $\boldsymbol{p}$, node $\boldsymbol{i}$ and node $\boldsymbol{j}$ in last step:

$$\begin{cases} \vec{F_{p-new}} = \vec{F_{p-old}} - \vec{F_g} \\ \vec{F_{i-new}} = \vec{F_{i-old}} + w_i \vec{F_g} \\ \vec{F_{j-new}} = \vec{F_{j-old}} + w_j \vec{F_g} \end{cases} \tag{24}$$

3. Precision test

3.1 Elastic analysis of rock under gravity load

The size of rock is 20 m × 20 m. The bottom boundary of rock is totally fixed, and the direction of gravity load is vertically downward. The density of rock is 2,000 kg/m^3, elastic modulus is 30 GPa, and Poisson's ratio is 0.25. For testing the robust of PCMM, three different PCMM models (particle-based) and one traditional FVM model (element-based) are used to represent this rock (Figure 7). Nine monitoring points with $X = 10$ m are set up for each model (Figure 7, red square denotes monitoring point). In regular PCMM model, particle radius is 0.5 m, particle number is 400 and contact searching tolerance $\boldsymbol{\delta}$ is 0.5 m. In cross PCMM model, particle radius is $\sqrt{3}/3$ m, particle number is 389 and contact searching tolerance $\boldsymbol{\delta}$ is 0.01 m. In random PCMM model, the random particles are generated by GiD (a pre and post processor), with the particle radius 0.168-0.312 m, particle number 1,966 and contact searching tolerance 0.3 m. In FVM element model, the element size is 1 m × 1 m, and element number is 400. Based

Downloaded by Kungliga Tekniska Högskolan At 00:52 26 February 2016 (PT)

Downloaded by Kungliga Tekniska Högskolan At 00:52 26 February 2016 (PT)

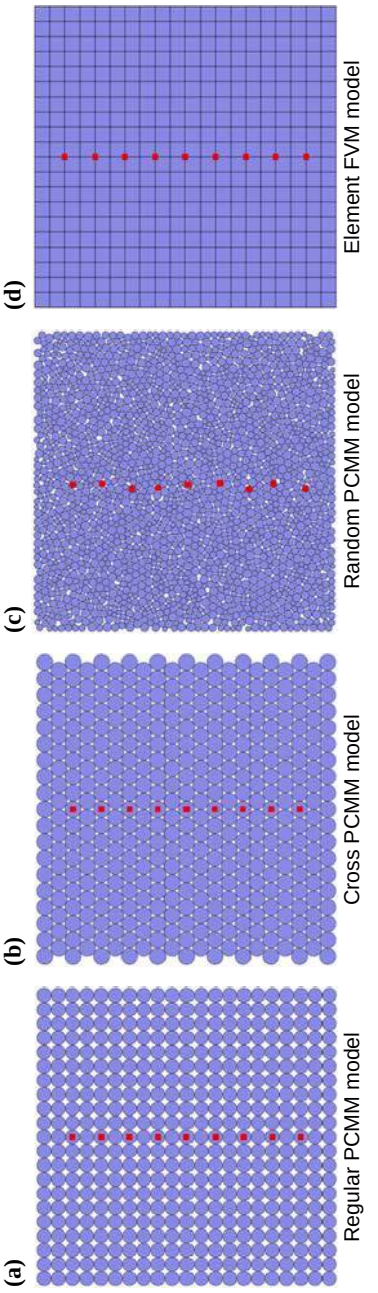

Figure 7.
Three PCMM models and one element model

on element creation algorithm mentioned in Section 2.2, three element systems related to regular model, cross model and random model are set up (Figure 8).

The relationship between vertical displacement and model height at $X = 10$ m are shown in Figure 9, and the relationship between vertical stress and model height at $X = 10$ m is shown in Figure 10. From Figures 9 and 10, the results of three different PCMM models are more or less the same as the element-based model, which shows the accuracy of PCMM. However, because X coordinate of monitoring points in random PCMM model (Figure 7(c)) do not equal 10 m exactly, the result of random model is slightly different from other three models.

3.2 Uniaxial compression of rock

The size of the rock sample is 0.1 m × 0.2 m, with bottom boundary totally fixed and top boundary horizontally fixed. To simulate quasi-static compression process, a small constant velocity is applied on the top boundary on vertical direction. For simulating the failure of the sample, Mohr-Coulomb criteria and maximum tensile criteria are adopted, with the density 2,500 kg/m^3, elastic modulus 30 GPa, Poisson's ratio 0.25, cohesion 3 MPa, tension 1 MPa, friction angle 40 degree.

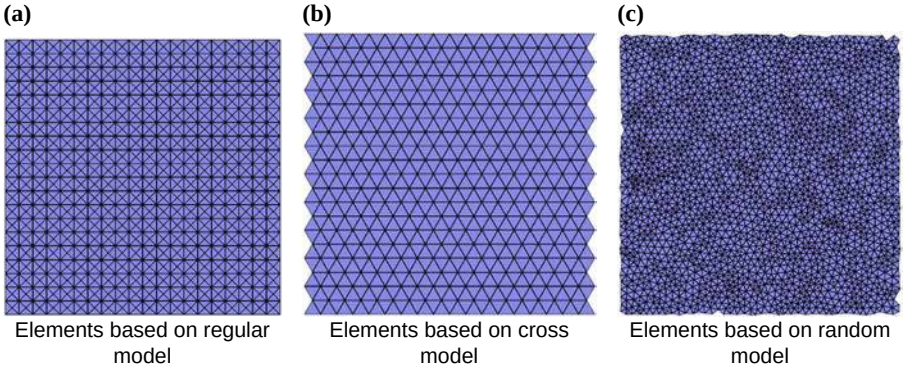

Figure 8.
Initial elements based on particle contacts in PCMM

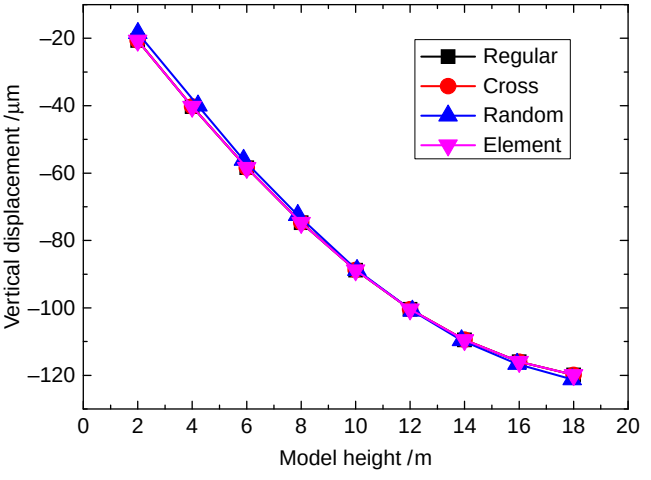

Figure 9.
Variation of vertical displacement with model height

Downloaded by Kungliga Tekniska Högskolan At 00:52 26 February 2016 (PT)

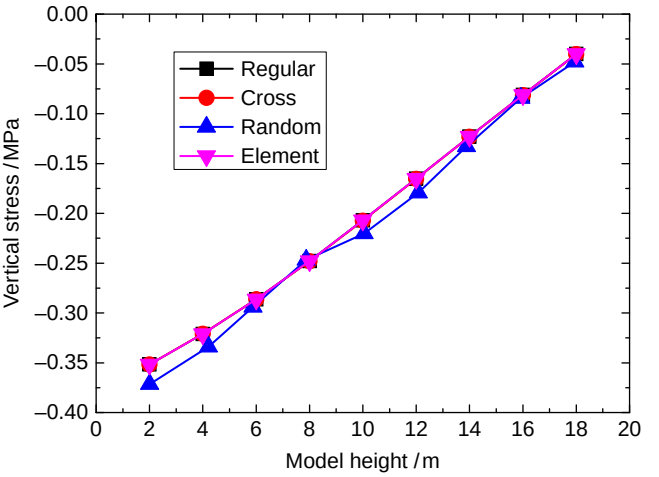

Figure 10.
Variation of vertical stress with model height

For testing the robust of PCMM, three different PCMM models and two different element-based FVM models are set up (Figure 11). In PCMM regular model, the particle radius is 2.5 mm, the particle number is 861 and contact searching tolerance $\boldsymbol{\delta}$ is 2.5 mm. In PCMM cross model, the particle radius is 2.5 mm, the particle number is 964 and contact searching tolerance $\boldsymbol{\delta}$ is 0.01 mm. In PCMM random model, the random particles are created by GiD, with the particle radius 1.09-2.02 mm, particle number 2,246 and contact searching tolerance 2.3 mm. In FVM regular model and FVM cross model, the element number are 800 and 1794, respectively. Based on element creating method mentioned in Section 2.2, different triangle element systems are created for regular, cross and random PCMM models (Figure 12).

The relationships between average stresses and strains of the five models are shown in Figure 13. From Figure 13, the behaviors of the five models in elastic stage are nearly the same, which demonstrates the robust of PCMM (little affection about particle arrangement). In plastic stage, grid type will affect the result to some extent. However, the results of particle regular model and element regular model are the same, and the results of particle cross model and element cross model are the same. The different behaviors in plastic stage show that, the gird type and style will affect the result, but with the same configuration, the results of PCMM and element-based FVM are the same.

3.3 Wave propagation in a rock bar

For testing the wave propagation in a rock bar, three different PCMM models and one element-based FVM model are set up (Figure 14), with the size 20 m × 0.6 m. Fixed boundary condition is applied on the right side, and dynamic sinusoidal velocity load is applied on the left side, with the amplitude 10 m/s, period 6 ms and time duration 3 ms. The density of this rock is 2,500 kg/m^3, elastic modulus is 30 GPa and Poisson's ratio is 0.25.

In regular PCMM model, the radius is 5 cm, the particle number is 1,206 and contact searching tolerance $\boldsymbol{\delta}$ is 5 cm. In cross PCMM model, the radius is 5 cm, particle number is 1,404 and contact searching tolerance $\boldsymbol{\delta}$ is 0.1 cm. In random PCMM model, the random particles are created by GiD, with the particle radius 1.39-4.23 cm, particle number 5,043 and contact searching tolerance 5 cm. In element FVM model, element size is 10 cm × 10 cm, and the element number is 1,200.

Downloaded by Kungliga Tekniska Högskolan At 00:52 26 February 2016 (PT)

Downloaded by Kungliga Tekniska Högskolan At 00:52 26 February 2016 (PT)

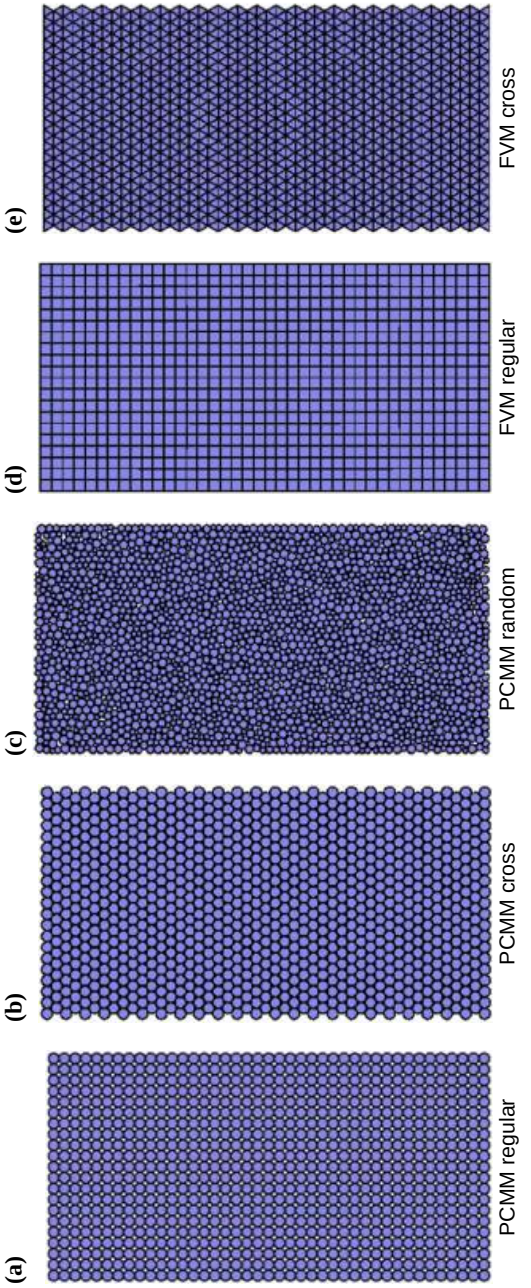

Figure 11.
Uniaxial
compression models

Downloaded by Kungliga Tekniska Högskolan At 00:52 26 February 2016 (PT)

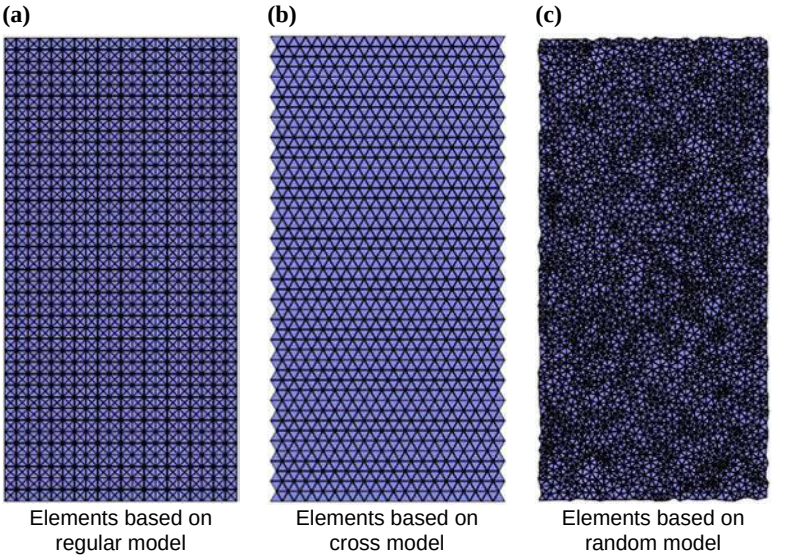

Figure 12.
Initial elements created by PCMM model

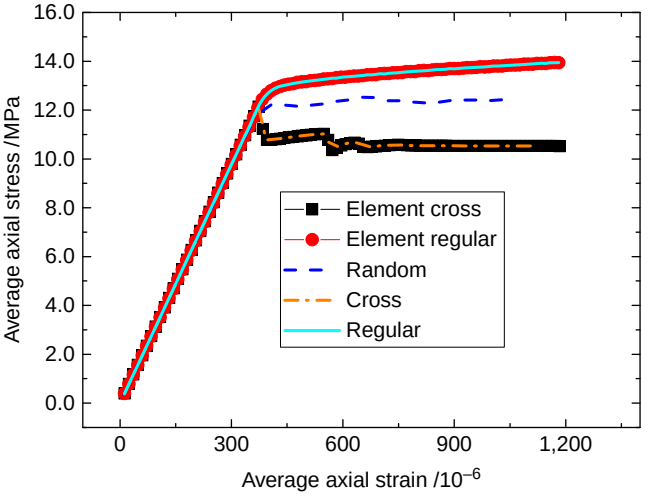

Figure 13.
Relationship between stress and strain in different models

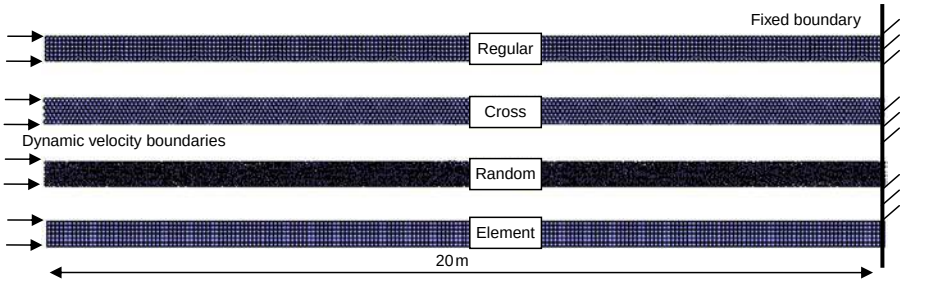

Figure 14.
Different models for rock bars

Velocity history curve and stress history curve at X = 10 m (middle point) are shown in Figures 15 and 16. From these two figures, time history curves of velocity and stress of four models are almost the same, which shows that PCMM could simulate dynamic problems well. However, particle arrangement will affect the result slightly, especially for the random PCMM model.

4. Geotechnical problems simulation

4.1 Soil cutting

The soil cutting numerical model is shown in Figure 17, and the size of soil is 3 m × 1 m, with bottom and right boundaries totally fixed. The blade consists of 375 triangle elements, and soil is formed by PCMM particles (7,701 particles with the radius 0.01 m

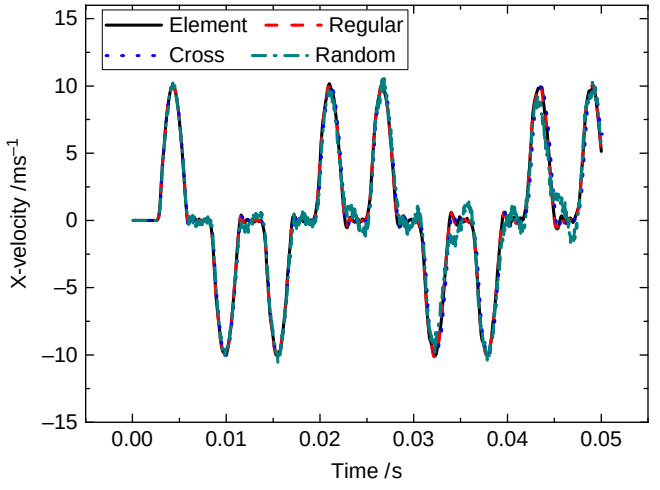

Figure 15.
Horizontal velocity history curve at X = 10 m

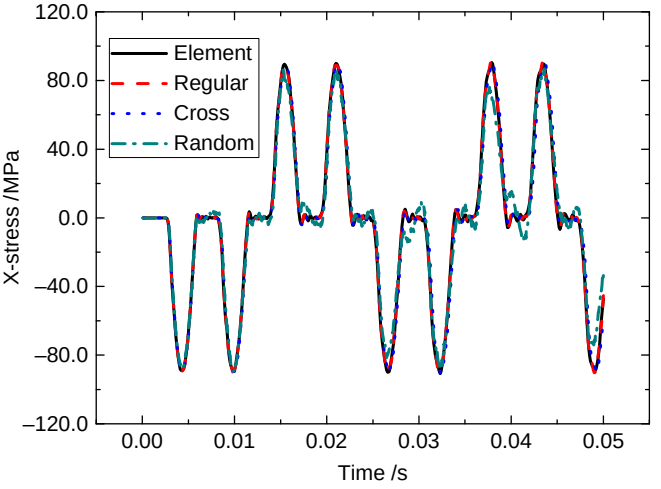

Figure 16.
Horizontal stress history curve at X = 10 m

Downloaded by Kungliga Tekniska Högskolan At 00:52 26 February 2016 (PT)

Downloaded by Kungliga Tekniska Högskolan At 00:52 26 February 2016 (PT)

and contact searching tolerance 0.01 m). Fixed horizontal velocity is applied on the left boundary of blade, with the value 0.1 m/s. Elastic model is used for blade, and Mohr-Coulomb model and maximum tensile model is used for soil. For the blade, the density is 7,800 kg/m^3, elastic modulus is 210 GPa and Poisson's ratio is 0.3. For the soil, the density is 1,750 kg/m^3, elastic modulus 10 MPa, Poisson's ratio 0.35, cohesion 10 kPa, inner friction angle 20 degree and tensile strength 3 kPa. Three points used to monitor vertical displacement are set on the top of the soil, with the name P1, P2 and P3, respectively. One point used to monitor bulk stress is set near the right and bottom side, with the name P4.

From Figure 18, when the blade moves toward to right-hand side gradually, the soil is separated by blade gradually, and some soil on the top of the blade will fall down due to the gravity load. At time 2 s, the first shear band forms basically; at time 6 s, the second shear band forms totally; and at time 11 s, the third shear band forms. From Figure 18, the distance between two adjacent shear bands is about 0.3 m. The evolvement of plastic shear band in soil when cutting shows the accuracy of PCMM.

The variations of vertical displacement and bulk stress with time on monitoring points are shown in Figures 19 and 20. From Figure 19, the displacement evolvements of these three points are more or less the same, and all of the displacements rise gradually and decline sharply. Vertical displacement of P1 rises at time 3.9 s, and reaches the peak at time 20 s, with the peak value 0.62 m, and then declines to −0.27 m

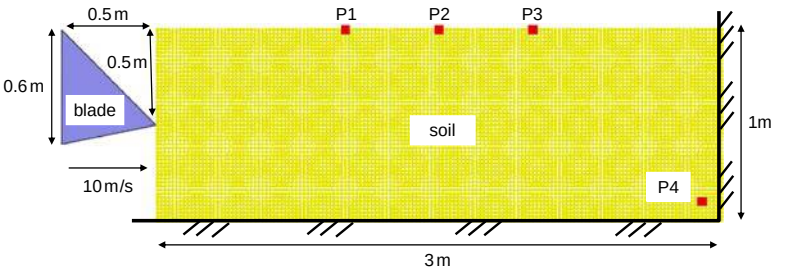

Figure 17.
Soil cutting model

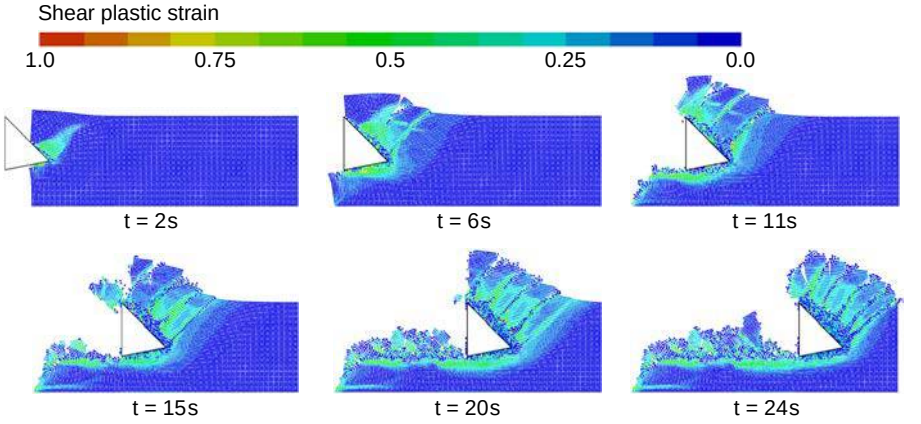

Figure 18.
Shear plastic strain of soil when cutting

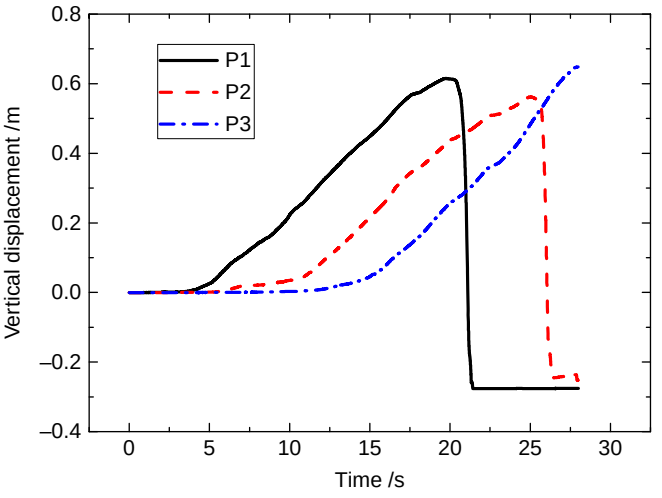

Figure 19.
Variation of vertical displacement with time

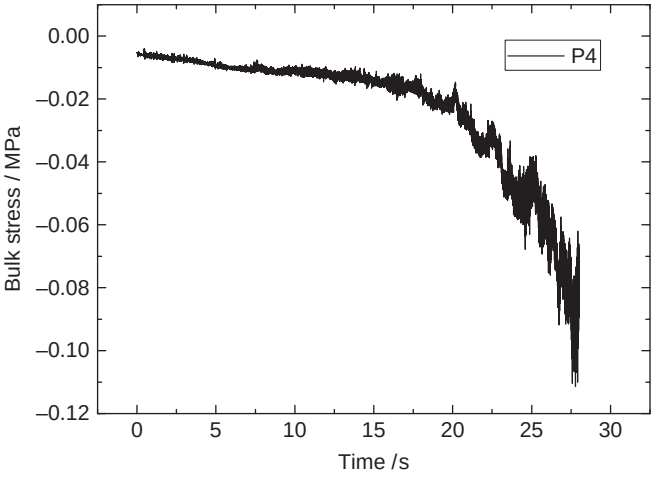

Figure 20.
Variation of bulk stress with time

quickly. From Figure 20, with the cutting time goes on, the bulk stress increases gradually. Before time 15 s, there is a slow and linear increase of bulk stress. After time 15 s, the bulk stress increases exponentially. At time 27.5 s, the bulk stress reaches −0.11 MPa.

4.2 Contact burst

For simulating contact burst, JWL model (Equation 25) is adopted for blasting source, where $\boldsymbol{P}$ is the pressure of explosive product, V' is the relative specific volume, $\boldsymbol{E}$ is the internal energy, and $\boldsymbol{A}$, $\boldsymbol{B}$, $\boldsymbol{R_1}$, $\boldsymbol{R_2}$ and $\boldsymbol{\omega}$ are experimental parameters. In this simulation, blasting source assumes as **TNT**, with $\boldsymbol{A} = 371.2$ GPa, $\boldsymbol{B} = 3.2$ GPa, $\boldsymbol{R_1} = 4.2$, $\boldsymbol{R_2} = 0.95$ and $\boldsymbol{\omega} = 0.3$. The blasting object assumes as soft rock, and Mohr-Coulomb model and maximum tensile model are used for this target, with density

Downloaded by Kungliga Tekniska Högskolan At 00:52 26 February 2016 (PT)

Downloaded by Kungliga Tekniska Högskolan At 00:52 26 February 2016 (PT)

2,500 kg/m^3, elastic modulus 20 GPa, Poisson's ratio 0.25, cohesion 0.1 MPa, tension 0.05 MPa, friction angle 30 degree:

$$p = A\left(1-\frac{\omega}{R_1 V'}\right)e^{-R_1 V} + B\left(1-\frac{\omega}{R_2 V'}\right)e^{-R_2 V} + \frac{\omega E}{V'} \tag{25}$$

The size of the numerical model is 8 m × 2 m, and the bottom, left and right boundaries of the model are all no reflection boundaries. Blasting source locates on the top of the model, with the charge radius 0.15 m. The numerical model consists of 40,501 PCMM particles, with the particle radius 0.01 m and contact tolerance 0.01 m. Three points named P1, P2 and P3 are set on the top right of the model to obtain the horizontal displacement history, and other three points named P4, P5 and P6 are set on the middle to monitor the pressure history (Figure 21).

After blasting, the pressure wave propagates to the soft rock gradually, and the value of pressure decreases gradually (Figure 22). From Figure 22, with the time goes on, the explosion crater becomes larger and larger. At time 3.6 ms, the top diameter of the crater is 1.4 m, and the depth of the crater is 0.35 m. The failure process of this soft rock demonstrates the rationality of PCMM.

The variation of horizontal displacement and pressure with time on monitoring points are shown in Figures 23 and 24. From Figure 23, the horizontal displacement of P1 increases linearly after time 0.46 ms, and then the displacements of P2 and P3 increase gradually. From Figure 24, the peak pressures of P4, P5 and P6 are 1,369 MPa, 931.8 MPa and 699.6 MPa, respectively.

4.3 Water-like material flowing

According to Equation (8), if $\boldsymbol{G} = 0$ and $\boldsymbol{K} = 2$ GPa, water-like material flowing could be simulated. The water and blocks interaction model is shown in Figure 25. The water is discretized by 5,528 PCMM particles, with the radius 3-8 mm and contact searching tolerance 5 mm. The size of the water is 0.8 m × 1.4 m, and the size of each block is 10 cm × 10 cm, the distance between right boundary of water and left boundary of blocks is 1.15 m. The contact properties between blocks are cohesion 0 MPa, inner friction angle 25 degree and tensile strength 0 MPa.

When the board on the right-hand side of water is removed, water will move toward to the block system gradually under gravity load. When water touches the block system, the blocks will begin to move under the water pressure. Two different block systems named four columns system and two columns system are set up to simulate the interaction between water and blocks, and the numerical results are shown in

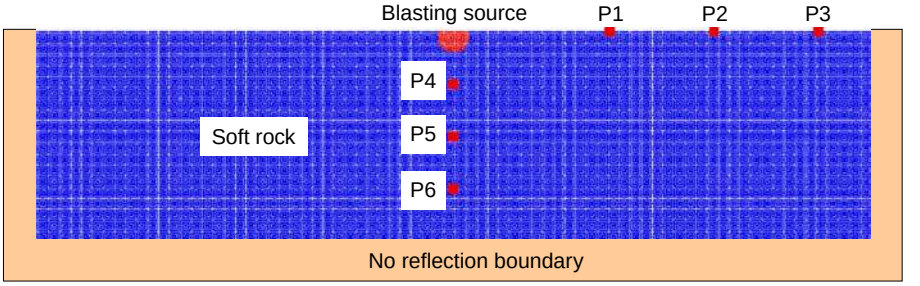

Figure 21.
Contact burst model

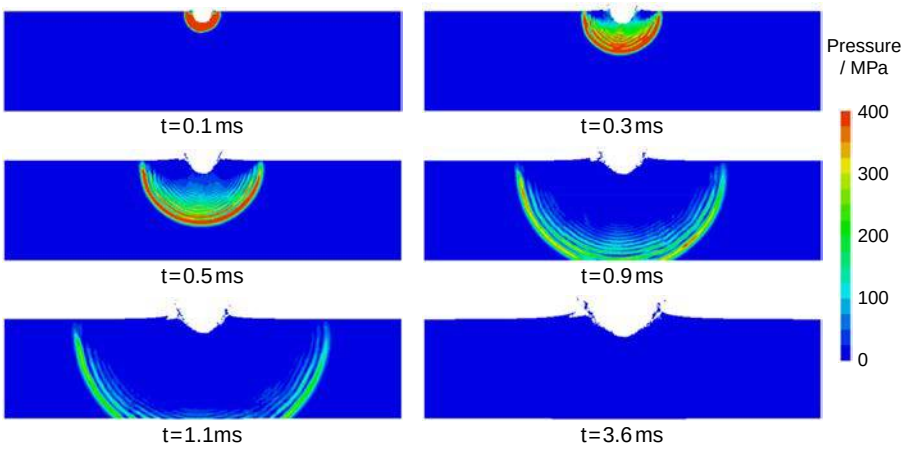

Figure 22.
Pressure wave propagation in soft rock

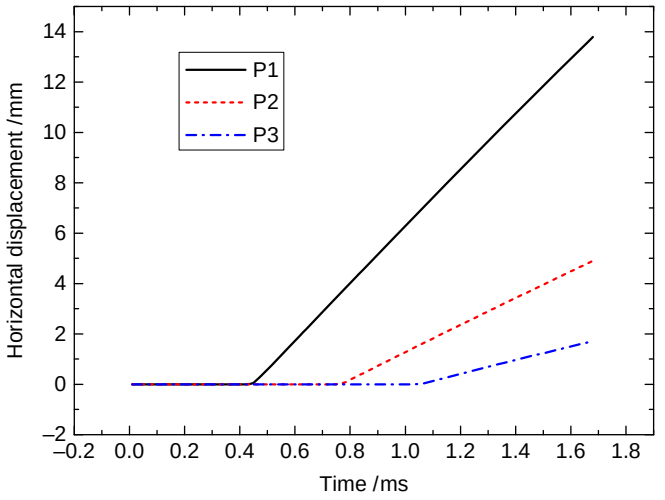

Figure 23.
Variation of horizontal displacement with time

Figures 26 and 27. From Figure 26, the impact action of water just causes little movement of blocks, and most of the water is confined to the left of block system. From Figure 27, block system topples to right-hand side under the impact of water, and the water occupies the bottom of sink. Different numerical results in these two figures show the correctness of PCMM.

5. Conclusions

PCMM is based on traditional particle DEM, and uses particle contacts to generate triangular elements. If three particles are contact with each other, the triangle element will be created. Once the elements are created, the macroscopic constitutive law could be introduced in. When large deformation of element occurs, the contact relationship between particles will be changed. Those elements that do not

Downloaded by Kungliga Tekniska Högskolan At 00:52 26 February 2016 (PT)

Downloaded by Kungliga Tekniska Högskolan At 00:52 26 February 2016 (PT)

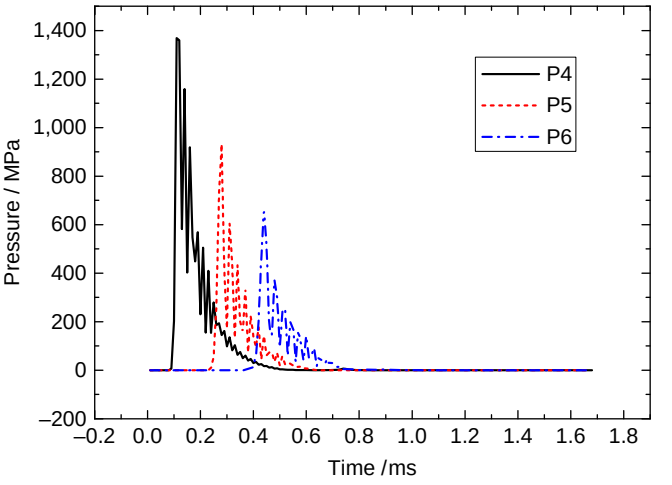

Figure 24.
Variation of pressure with time

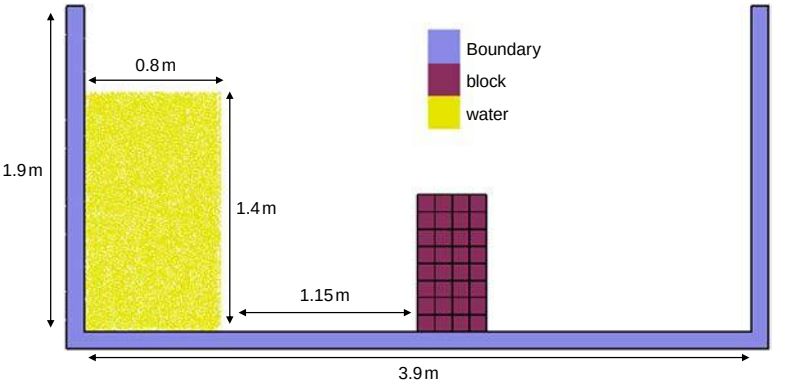

Figure 25.
Water and block interaction model

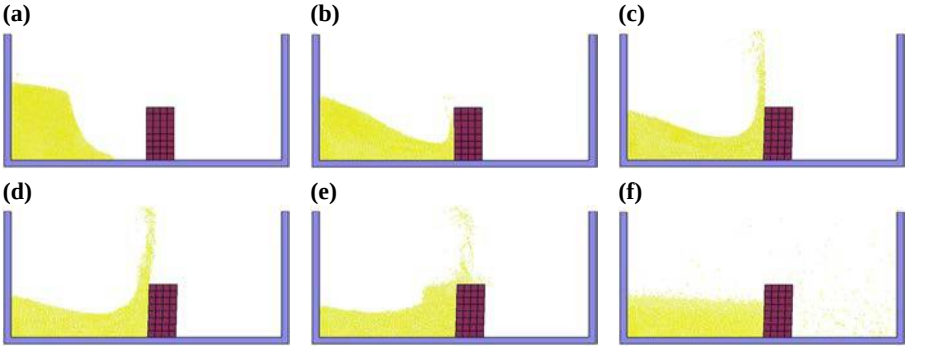

Figure 26.
Four columns block system: this figure shows the movement of four columns block system under water impacting load. From (a) to (f), the physical time is 0.36s, 0.68s, 0.96s, 1.28s, 1.84s, 4.08s, respectively

Downloaded by Kungliga Tekniska Högskolan At 00:52 26 February 2016 (PT)

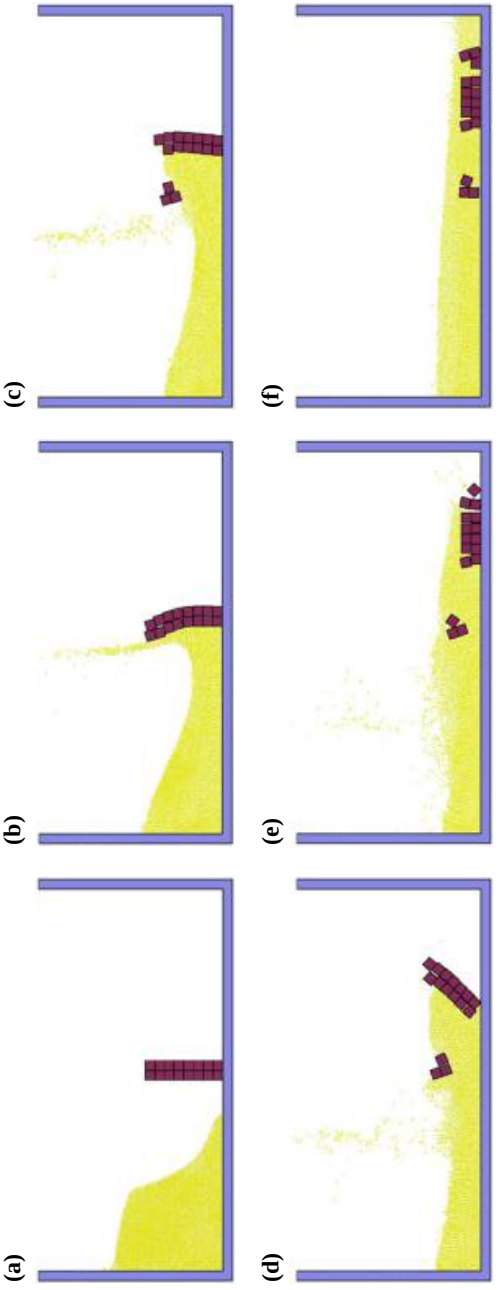

Figure 27.
Two columns block system: this figure shows the movement of two columns block system under water impacting load. From (a) to (f), the physical time is 0.40s, 0.88s, 1.28s, 1.72s, 2.08s and 4.76s, respectively

meet the contact conditions will be deleted and new elements that coincide with the relationships will be generated. According to the deletion and recreation of the elements by particle contacts, PCMM could simulate large deformation problems. Some numerical cases (i.e. elastic field testing, uniaxial compression analysis and wave propagation simulation) show the accuracy of PCMM, and others (i.e. soil cutting, contact burst and water-like material flowing) show the rationality of PCMM.

However, PCMM requires more validation, such as the selection of contact searching tolerance, principles to create or delete elements and approaches of information transformation between particles and elements.

Downloaded by Kungliga Tekniska Högskolan At 00:52 26 February 2016 (PT)

References

Ambati, R., Pan, X.F., Yuan, H. and Zhang, X. (2012), "Application of material point methods for cutting process simulations", *Computational Materials Science*, Vol. 57, pp. 102-110.

Brackbill, J.U. and Ruppel, H.M. (1986), "Flip: a method for adaptively zoned, particle-in-cell calculations in two dimensions", *Journal of Computational Physics*, Vol. 65 No. 2, pp. 314-343.

Campbell, P.M. (1989), "Some new algorithms for boundary value problems in smoothed particle dynamics", Technical Report of Defense Nuclear Agency, Washington, DC, No. ADA211728, pp. 1-48, available at: http://oai.dtic.mil/oai/oai?verb=getRecord&metadataPrefix=html&identifier=ADA211728

Chen, J.K., Beraun, J.E. and Jih, C.J. (1999), "An improvement for tensile instability in smoothed particle hydrodynamics", *Computational Mechanics*, Vol. 23 No. 4, pp. 279-287.

Cleary, P.W., Ha, J., Prakash, M. and Nguyen, T. (2006), "3D SPH Flow predictions and validation for high pressure die casting of automotive components", *Applied Mathematical Modelling*, Vol. 30 No. 11, pp. 1406-1427.

Dyka, C.T., Randles, P.W. and Ingel, R.P. (1997), "Stress points for tension instability in SPH", *International Journal for Numerical Methods in Engineering*, Vol. 40 No. 13, pp. 2325-2341.

Gingold, R.A. and Monaghan, J.J. (1977), "Smoothed particle hydrodynamics: theory and application to non-spherical stars", *Monthly Notices of the Royal Astronomical Society*, Vol. 181 No. 3, pp. 375-389.

Jing, L.R. and Stephansson, O. (2007), *Fundamentals of Discrete Element Methods for Rock Engineering Theory and Applications*, Amsterdam, Elsevier.

Li, S.H., Zhao, M.H., Wang, Y.N. and Rao, Y. (2004), "A new numerical method for DEM-block and particle model", *International Journal of Rock Mechanics and Mining Sciences*, Vol. 41 No. 3, p. 436.

Li, S.H., Wang, J.G., Liu, B.S. and Dong, D.P. (2007), "Analysis of critical excavation depth for a jointed rock slope by face-to-face discrete element method", *Rock Mechanics and Rock Engineering*, Vol. 40 No. 4, pp. 331-348.

Littlefield, D.L. (2001), "The use of r-adaptivity with local, intermittent remesh for modeling hypervelocity impact and penetration", *International Journal of Impact Engineering*, Vol. 26 Nos 1-10, pp. 433-442.

Liu, W.K., Belytschko, T. and Chang, H. (1986), "An arbitrary Lagrangian-Eulerian finite element method for path-dependent materials", *Computer Methods in Applied Mechanics and Engineering*, Vol. 58 No. 2, pp. 227-245.

Liu, W.K., Chen, J.S., Belytschko, T. and Zhang, Y.F. (1991), "Adaptive ALE finite elements with particular reference to external work rate on frictional interface", *Computer Methods in Applied Mechanics and Engineering*, Vol. 93 No. 2, pp. 189-216.

Lucy, L.B. (1977), "A numerical approach to the testing of the fission hypothesis", *Astronomical Journal*, Vol. 82 No. 12, pp. 1013-1024.

Ma, G.W., Wang, X.J. and Ren, F. (2011a), "Numerical simulation of compressive failure of heterogeneous rock-like materials using SPH method", *International Journal of Rock Mechanics & Mining Sciences*, Vol. 48 No. 3, pp. 353-363.

Ma, S., Zhang, X. and Qiu, X.M. (2009), "Comparison study of MPM and SPH in modeling hypervelocity impact problems", *International Journal of Impact Engineering*, Vol. 36 No. 2, pp. 272-282.

Ma, Z.S., Feng, C., Liu, T.P. and Li, S.H. (2011b), "A GPU accelerated continuous-based discrete element method for elastodynamics analysis", *Advanced Materials Research*, Vol. 320, pp. 329-334.

Michel, Y., Chevalier, J.M., Durin, C., Espinosa, C., Malaise, F. and Barrau, J.J. (2006), "Hypervelocity impacts on thin brittle targets: experimental data and SPH simulations", *International Journal of Impact Engineering*, Vol. 33 Nos 1-12, pp. 441-451.

Monaghan, J.J. (2000), "SPH without a tensile instability", *Journal of Computational Physics*, Vol. 159 No. 2, pp. 290-311.

Oñate, E., Idelsohn, S.R., Del Pin, F. and Aubry, R. (2004), "The particle finite element method. An overview", *International Journal of Computational Methods*, Vol. 1 No. 2, pp. 267-307.

Randles, P.W. and Libersky, L.D. (2000), "Normalized SPH with stress points", *International Journal for Numerical Methods in Engineering*, Vol. 48 No. 10, pp. 1445-1462.

Sulsky, D., Chen, Z. and Schreyer, H.L. (1994), "A particle method for history-dependent materials", *Computer Methods in Applied Mechanics and Engineering*, Vol. 118 Nos 1-2, pp. 179-196.

Sulsky, D., Zhou, S.J. and Schreyer, H.L. (1995), "Application of a particle-in-cell method to solid mechanics", *Computer Physics Communications*, Vol. 87 Nos 1-2, pp. 236-252.

Swegle, J.W., Hicks, D.L. and Attaway, S.W. (1995), "Smoothed particle hydrodynamics stability analysis", *Journal of Computational Physics*, Vol. 116 No. 1, pp. 123-134.

Wang, Y.N., Zhao, M.H., Li, S.H. and Wang, J.G. (2005), "Stochastic structural model of rock and soil aggregates by continumm-based discrete element method", *Scinece in China Series E-Engineering & Materials Science*, Vol. 48 No. S1, pp. 95-106.

Corresponding author
Dr Chun Feng can be contacted at: fengchun@imech.ac.cn

Downloaded by Kungliga Tekniska Högskolan At 00:52 26 February 2016 (PT)

For instructions on how to order reprints of this article, please visit our website:
www.emeraldgrouppublishing.com/licensing/reprints.htm
Or contact us for further details: **permissions@emeraldinsight.com**